

Frequency-Domain System Identification of an Unmanned Helicopter Based on an Adaptive Genetic Algorithm

Yuhu Du, Jiancheng Fang, *Member, IEEE*, and Cunxiao Miao

Abstract—This paper presents a frequency-domain identification method for an unmanned helicopter (UH) based on an adaptive genetic algorithm (AGA). By using a homemade micro-guidance, navigation, and control system (MGNCS), data regarding the inputs (control signals of servos) and outputs (states of the UH) are recorded. After data preprocessing, the attitude model of the UH is identified by employing the AGA. The identified model is then analyzed in the time domain and the frequency domain in comparison with the least squares (LS) method. Control compensators are designed based on the identified model. Automatic hovering is successfully achieved based on the compensators. Simulation and experimental results demonstrate the effectiveness and superiority of this identification method.

Index Terms—Adaptive genetic algorithm (AGA), least squares (LS), system identification, unmanned helicopter (UH).

I. INTRODUCTION

UNMANNED aerial vehicles (UAVs) have been designed for applications in many areas for decades [1]–[3]. Among UAVs, the unmanned helicopter (UH) is an excellent aerial platform because it is able to take off and land vertically, cruise at ultra low speeds, and hover in the air. It has already drawn intensive attention worldwide for its distinguished features [4]–[10]. The UH has been successfully employed in civil and military applications, such as aeronautic photography, forest fire extinguishing and power line inspection, surveillance, battleground monitoring, etc.

As we know, the UH is a multivariable, nonlinear, and strongly coupled system, which brings great motivation for the modeling of the UH [11]. System identification, which is an

effective modeling technique that uses experimental input–output data to produce a mathematical model for the plant [12], has become an important approach through which to obtain dynamics parameters, which are useful for computer simulation and outdoor flight control experiments. In comparison with the wind tunnel approach, system identification is relatively low cost and easy to implement. In addition, in comparison with analytical methods, it is more direct because it is based on real input–output test data and is closer to reality.

In recent years, there has been increasing interest in the study of system identification methods for UAVs, mainly including time-domain and frequency-domain methods. Time-domain system identification is widely used to obtain dynamic models, and commonly used approaches include the least squares (LS) method [13]–[15], the prediction error method (PEM) [16]–[19], etc. Under the assumption that a loitering helicopter could be treated as a system with three independent single-input single-output (SISO), Park *et al.* [13] used LS to develop a new autoregressive model that corresponds to a three-degree-of-freedom (DOF) helicopter. Based on the flight test data, Wu *et al.* [14] identified two fourth-order autoregressive with exogenous input models, which present the attitude characteristics of the longitudinal (pitch) and the lateral (roll) control channels, respectively. Cai *et al.* [16] adopted PEM to minimize the sum of squared prediction errors at all sample points, and compared the identified model with the actual measured frequency response. Manai *et al.* [20] identified the parameters of the nonlinear model of a manned aerial vehicle based on the output error approach for the purpose of replacing an existent gain-scheduled proportional–integral–derivative with a nonlinear controller.

Although time-domain methods are widely employed to obtain the dynamic models of UAVs, regarding the system identification of the UH, frequency-domain methods are more suitable than time-domain methods due to their high-grade properties [21]. Frequency-domain identification is manipulated by minimizing a frequency-domain cost function. Due to the prespecified frequency range estimated from the frequency response of input–output data, irrelevant information, such as noise and disturbance, are separated from the information that is relevant to the system identification of the UH dynamic model. Moreover, output measurement noise and process noise are automatically separated from the data. Therefore, this type of disturbance does not bias the frequency response

Manuscript received January 31, 2012; revised June 1, 2012, September 3, 2012, November 6, 2012, and January 28, 2013; accepted March 16, 2013. Date of publication April 5, 2013; date of current version August 9, 2013. This work was supported in part by the National Outstanding Youth Fund of China under Grant 60825305, in part by the National Basic Research Program of China under Grant 2009CB72400101C, in part by the National Natural Science Foundation of China under Grant 61273033, and in part by the Beijing Municipal Natural Science Foundation under Grant 4132043.

Y. Du and J. Fang are with the Science and Technology on Inertial Laboratory, and the Fundamental Science on Novel Inertial Instrument and Navigation System Technology Laboratory, School of Instrumentation Science and Optoelectronics Engineering, Beihang University, Beijing 100083, China (e-mail: duyuhu@aspe.buaa.edu.cn; fangjiancheng@buaa.edu.cn).

C. Miao is with the School of Mechanical Engineering, University of Science and Technology Beijing, Beijing 100083, China (e-mail: miao_cunxiao@163.com).

Color versions of one or more of the figures in this paper are available online at <http://ieeexplore.ieee.org>.

Digital Object Identifier 10.1109/TIE.2013.2257135



Fig. 1. UH.

TABLE I
PARAMETERS OF THE UH

Length	1410 mm
Height	630 mm
Diameter of Main Rotor	1610 mm
Diameter of Tail Rotor	265 mm
Payload	3 Kg

estimate. Comprehensive Identification from Frequency Response (CIFER), which was developed by the U.S. Army and NASA, and has become a common tool used for frequency-domain identification, has been successfully used in a wide range of fixed, rotary-wing, and unconventional aircraft applications [22]–[27]. By using CIFER, Mettler *et al.* [23]–[26] derived a linear state-space model for a small-scale UH in the hovering condition. Nino *et al.* [27] used CIFER to identify the lateral and longitudinal SISO models for a micro air vehicle.

As we know, a genetic algorithm (GA) is based on the mechanism of natural evolution and population genetics. As a robust and efficient searching algorithm, it is widely used to identify the parameters of models [28]–[30]. In this paper, we intend to identify the model of the UH using the frequency-domain method and utilize the adaptive GA (AGA) to obtain the optimal parameters of the dynamic model for its high searching performance.

This paper is organized as follows. In Section II, the dynamic model of the system is reviewed, and a discrete transfer function model for the attitude rate is presented. An AGA identification method is presented in Section III. In Section IV, the AGA is utilized to fine-tune the parameters of the dynamic model based on the actual flight data. Verification of frequency and time domains, as well as flight control experiments, is implemented to test the validity of the identified model in Section V. Finally, conclusions are provided in Section VI.

II. SYSTEM DYNAMIC MODEL

As shown in Fig. 1, the UH used in this paper is upgraded from a radio-controlled hobby helicopter. The physical parameters of the UH are depicted in Table I. The UH is powered by a piston engine running on a mixed-model engine fuel.

The UH is free to rotate and translate in the air. Fig. 2 shows the key forces acting on the six-DOF UH [23]. Origin O is the

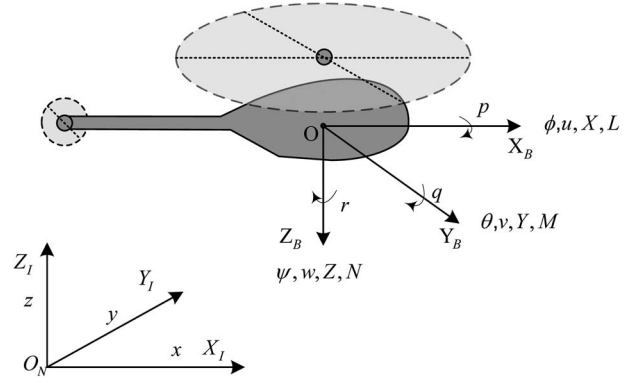


Fig. 2. Forces and moments acting on the UH.

center of gravity of the UH, and X_B , Y_B , and Z_B form the body reference frame; u , v , and w are the velocities in the X_B , Y_B , and Z_B directions, respectively; ϕ , θ , and ψ are the Euler angles; p , q , and r are the angular rates along the X_B , Y_B , and Z_B axes, respectively; X , Y , and Z are the forces acting on the center of gravity of the UH, whereas L , M , and N are the moments in X_B , Y_B , and Z_B , respectively; and x , y , and z form the displacement of the center of gravity of the UH from O_I in the X_I , Y_I , and Z_I axes of the inertial frame, respectively.

In order to obtain the dynamic model of the UH, we make the following assumptions.

- 1) The UH is a rigid body.
- 2) The UH is symmetric.
- 3) The mass distribution of the UH is unchanged during the flight.
- 4) The cross product of inertia is small; therefore, the principal axes are coincident with the axes of the body reference system.

Then, based on Newton's second law and the principle of rotor dynamics, the translational and rotational motion equations that describe the UH in the hovering condition can be described as

$$\begin{cases} m \left(\frac{du}{dt} + wq - vr \right) = X \\ m \left(\frac{dv}{dt} + ur - wp \right) = Y \\ m \left(\frac{dw}{dt} + vp - uq \right) = Z \end{cases} \quad (1)$$

$$\begin{cases} I_x \frac{dp}{dt} + (I_z - I_y)qr = L \\ I_y \frac{dq}{dt} + (I_x - I_z)rp = M \\ I_z \frac{dr}{dt} + (I_y - I_x)pq = N \end{cases} \quad (2)$$

where m is the mass of the UH, and I_x , I_y , and I_z are the moments of inertia of the UH in the X_B , Y_B , and Z_B axes, respectively. With the equations in (1) and (2), we can yield the model of the UH in different structures, e.g., a state-space model or a transfer function model. In this paper, we intend to identify the transfer function of the attitude channel of the UH. A previously obtained model [21], [23] is introduced here, whose transfer function is given by

$$\begin{cases} \frac{p}{\delta_{\text{lat}}} = \frac{L_a A_{\text{lat}} / \tau_f}{s^2 + (1/\tau_f)s + L_a} \\ \frac{q}{\delta_{\text{lon}}} = \frac{L_b A_{\text{lon}} / \tau_f}{s^2 + (1/\tau_f)s + L_b} \end{cases} \quad (3)$$

where δ_{lat} and δ_{lon} are the lateral cyclic control input and the longitudinal cyclic control input, respectively; L_a is the lateral rotor moment derivative; A_{lat} is the parameter of the lateral stick to cyclic pitch gearing; L_b is the longitudinal rotor moment derivative; A_{lon} is the parameter of the longitudinal stick to cyclic pitch gearing; and τ_f is the main rotor time constant.

The cyclic control input of the UH is controlled by the servo installed on the UH, whose model can be described as a first-order inertia term, i.e.,

$$\frac{\delta}{u} = \frac{1}{1 + T_\delta s} \quad (4)$$

where u is the input of the servo, δ is the output, and T_δ is the time constant.

According to (3) and (4), the relationship between the attitude rate and the input of the servo actuator can be obtained

$$\begin{cases} \frac{p}{u_{\text{lat}}} = \frac{L_a A_{\text{lat}} / \tau_f}{s^2 + (1/\tau_f)s + L_a} \cdot \frac{1}{1 + T_\delta s} \\ \frac{q}{u_{\text{lon}}} = \frac{L_b A_{\text{lon}} / \tau_f}{s^2 + (1/\tau_f)s + L_b} \cdot \frac{1}{1 + T_\delta s} \end{cases} \quad (5)$$

where u_{lat} and u_{lon} are the inputs of the servos of the lateral channel and the longitudinal channel, respectively.

III. AGA

In this section, we will introduce the flowchart of the AGA employed in this paper, and the key components of the AGA will be also depicted in detail.

A. Algorithm Flowchart

The flowchart for the AGA is shown in Fig. 3. The AGA begins by defining an array of chromosomes (i.e., individuals) to be evaluated. Because the experimental data obtained are discrete, a bilinear transformation is utilized to obtain the discrete model of the UH for the sake of model verification in Section V. The discrete model of the UH derived from (5) is shown as follows:

$$\begin{cases} \frac{p}{u_{\text{lat}}} = \frac{b_1 z^3 + b_2 z^2 + b_3 z + b_4}{z^3 + a_1 z^2 + a_2 z + a_3} \\ \frac{q}{u_{\text{lon}}} = \frac{d_1 z^3 + d_2 z^2 + d_3 z + d_4}{z^3 + c_1 z^2 + c_2 z + c_3} \end{cases} \quad (6)$$

According to (6), in the process of identification of the lateral channel, each chromosome has seven variables. The chromosome uses real number encoding and is written as an array with 1×7 elements, as follows:

$$\text{chromosome} = [a_1, a_2, a_3, b_1, b_2, b_3, b_4]. \quad (7)$$

A similar equation can be obtained for the longitudinal channel.

In this paper, the LS is utilized as a time-domain method [31]. It is employed to minimize the sum of the squares of the errors between the observed values and the fitted values provided by the model. At the beginning of the process of identification, the LS method is utilized to get the initial solution, and the corresponding search spaces should be established to avoid blind exploration and to improve the efficiency of the identification. The AGA then is developed to obtain an improved solution. In

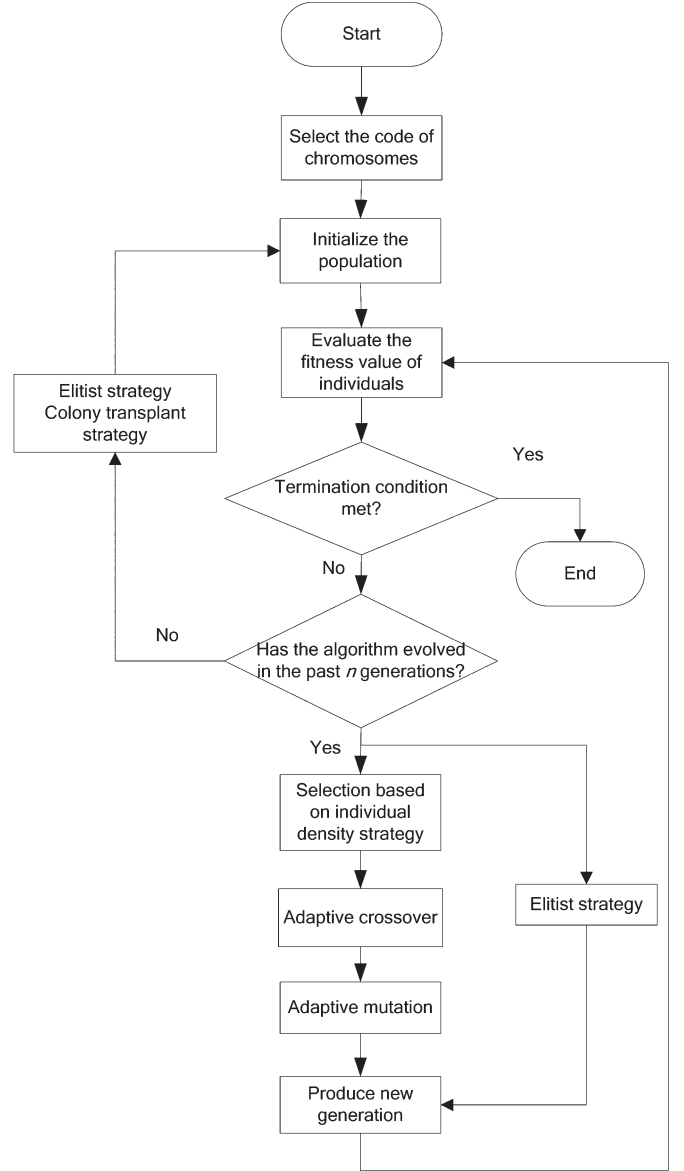


Fig. 3. Flowchart of the AGA.

the searching spaces of the AGA, the individuals of the first generation are established, with each individual representing a model.

After the analysis of the frequency response errors between the real test data and the candidate models, the individuals are given different fitness values. The individuals with high fitness values tend to be selected as parents to generate offspring by using adaptive crossover and mutation operations. The AGA moves from generation to generation to select suitable solutions until the termination constraints are met.

Finally, the best individual with the maximum fitness value is found, i.e., the optimal result of the dynamic model of the UH.

B. Fitness Function

The fitness function, which establishes a performance measurement criterion for the individuals of the AGA, plays an important role in the evolution process. Here, we use the

frequency response error as the evaluation criterion. The fitness function is defined as follows:

$$F(\Theta) = 1 \left/ \left[1 + \sum_{i=1}^N \varepsilon(\omega_i, \Theta)^T \varepsilon(\omega_i, \Theta) \right] \right. \quad (8)$$

where Θ is the candidate model (i.e., individual) in the AGA to be evaluated; ω_i is the sample frequency point; N is the number of sample frequency points; and $\varepsilon(\omega_i, \Theta)$ is the vector of the amplitude and phase error between the candidate model and the collected flight data. According to [21], the importance of the amplitude relative to the phase is specified as 20 dB to 57.3°. The accuracy of the identified model depends on the fitness function. The higher the fitness value is, the better the model will be.

C. Adaptive Crossover Operation

In the AGA, crossover is an operation to exchange some parts of two chromosomes. It can create new individuals by swapping segments of parent genetic information. The crossover operation used in the AGA is arithmetic crossover [32]. If the crossover rate is 100%, all offspring are generated by crossover. If the crossover rate is 0%, a whole new generation is made from exact copies of chromosomes from the old population. Crossover is made in the hope that new and improved chromosomes will emerge in the next generation. However, it is good to allow some part of the old population to survive to the next generation [33]. To improve the search performance, an adaptive crossover strategy is used. The adaptive crossover operator is defined as

$$P_c = \begin{cases} P_{c1} - \frac{(P_{c1}-P_{c2})(F'-F_{\text{avg}})}{F_{\text{max}}-F_{\text{avg}}}, & F' \geq f_{\text{avg}} \\ P_{c1}, & F' < f_{\text{avg}} \end{cases} \quad (9)$$

where P_c is the crossover rate; F_{max} and F_{avg} are the maximum fitness value and the average fitness value of the current generation, respectively; F' is the higher fitness value between the two individuals; and P_{c1} and P_{c2} are the preset crossover rates. P_{c1} , P_{c2} are constant parameters predefined by users.

On one hand, if F' is higher than the average fitness value of the current generation, the system will use the lower crossover rate to reduce the possibility of destruction in the evolution process. On the other hand, if F' is lower than the average fitness value of the current generation, the system adopts the higher crossover rate.

D. Adaptive Mutation Operation

Mutation is the operation used to change a part of the chromosome. The mutation operation used in the AGA is Gaussian mutation [33]. If the mutation rate is too high, the GA becomes a random searching algorithm with low searching performance. However, a low mutation rate may cause low production of the new population. To ensure the searching ability, an adaptive mutation strategy is used here. The mutation operator of the individual i is defined as

$$P_{mi} = \begin{cases} P_{m1} - \frac{(P_{m1}-P_{m2})(F_{\text{max}}-F)}{F_{\text{max}}-F_{\text{avg}}}, & F \geq F_{\text{avg}} \\ P_{m1}, & F < F_{\text{avg}} \end{cases} \quad (10)$$

where P_{mi} is the mutation rate, F is the fitness value of the current individual, and P_{m1} and P_{m2} are the mutation rates. P_{m1} and P_{m2} are constant parameters predefined by the user.

It is shown in (10) that, when the fitness value of an individual is higher than the average fitness value of the current generation, the system will adopt the lower mutation rate, and when the fitness value of the individual is lower than the average fitness value of the current generation, the system adopts the higher mutation rate.

E. Selection Operation Based on Individual Density Strategy

To select high-quality individuals and ensure their diversity, an individual density strategy is utilized here.

First, we define the density of individual i as follows:

$$A_i = \frac{l}{M} \quad (11)$$

where M is the number of individuals in the current generation, and l is the number of individuals whose fitness values satisfy

$$|F_j - F_i| \leq \delta \quad (12)$$

where $0 < \delta < 1$, F_i is the fitness value of individual i , and F_j is the fitness value of the individual in the current generation, except for individual i .

We then choose the individuals whose A_i is higher than a preset numerical value ε , which satisfies the following constraint:

$$0 < \varepsilon < 1. \quad (13)$$

The density probability of the individuals chosen is expressed as [34]

$$p_{t(m)} = \frac{1}{M} \left(1 - \frac{m}{M} \right) \quad (14)$$

where m is the number of the individuals whose A_i is higher than ε .

The density probability of the individuals whose A_i is lower than ε is expressed as

$$p_{t(M-m)} = \frac{1}{M} + \frac{m}{M^2(M-m)}. \quad (15)$$

For the sake of calculating the probability of selection of the individuals, we also define variable p_F , i.e., the fitness probability of the individual, which is shown in the following:

$$p_{F(i)} = \frac{F_i}{\sum_{j=1}^M F_j}. \quad (16)$$

Finally, the probability of selection of the individuals in the AGA can be calculated as follows:

$$p_{s(i)} = \alpha \cdot (\beta N_i + (1-\beta)p_{F(i)}) + (1-\alpha) \cdot (1-p_{t(i)}) \quad (17)$$

where p_s is the probability of selection; α and β are preset proportion factors, which satisfy $0 < \alpha$ and $\beta < 1$; and N_i is defined as

$$N_i = \frac{n_i}{M} \quad (18)$$

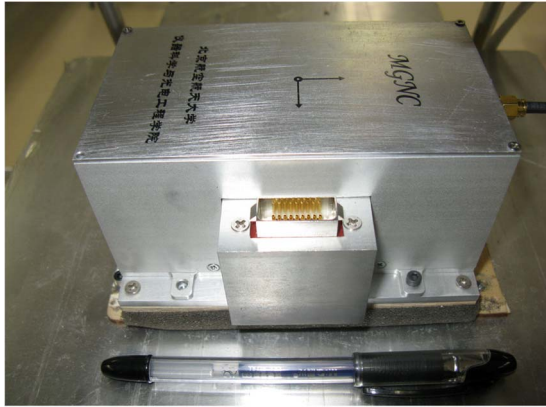


Fig. 4. MGNCs.

where n_i is the order of the individual's fitness value in the current generation. α and β determine the importance of N_i , $p_{F(i)}$, and $p_{t(i)}$.

As shown in (17), the higher the fitness value is, the higher the probability that the individual will be selected. We can also see that the higher the density of an individual, the lower the probability of selection. After the probability of selection is computed, the roulette wheel selection method is applied to the selection process. By virtue of the density strategy, individuals with high fitness values are encouraged, and at the same time, individuals with high-density probability are restrained, to ensure the diversity of individuals and to avoid the prematurity of the AGA.

To ensure system searching performance and convergence, the best individual in the population (i.e., the individual with the maximum fitness value) passes to the next generation without any modifications. In addition, the colony transplant strategy is adopted, i.e., when the algorithm does not evolve within a certain number of generations, the individuals will be regenerated. In the process of regeneration, the best individual is preserved. In this paper, when the GA fails to evolve for 100 generations, the colony transplant strategy is employed. The colony transplant strategy can improve the efficiency of the AGA and increase the probability of finding the optimal individual.

IV. IMPLEMENTATION OF IDENTIFICATION

A. Experimental Equipment

In order to implement the model identification, a series of flight experiments are needed to be carried out on the UH to acquire the corresponding input–output data. In previous years, we have designed several microguidance, navigation, and control systems (MGNCs) [35] based on the microelectromechanical systems (MEMS) and integrated navigation technologies [36]–[38]. Based on the previous versions, an upgraded version of the MGNCs (see Fig. 4) was designed for the experimental tests with the UH.

Due to constraints on the weight and size of the onboard components of the UH, the MGNCs weighs only 207 g, with a dimension of 120 mm \times 61 mm \times 48 mm. Fig. 5 shows the block diagram of the MGNCs, which consists of four

subsystems: data collection, navigation solution, flight control, and manual/autonomous mode transfer. Among the four components, the data collection subsystem consists of micro inertial measurement units (MIMUs), an ultrasonic sensor, a barometric altimeter, and a microprocessor, and it can collect information including that relating to inertia and altitude. The MIMU is composed of three MEMS gyros and accelerometers, and it can detect the angular rates and translational accelerations along three body axes. Information from the data collection subsystem and from the Global Positioning System receiver and the micromachined magnetic compass is fed into the navigation subsystem. Then, the data fusion algorithm, e.g., the Kalman filter, is utilized to acquire the real-time attitudes, attitude rates, position, velocities, etc.

B. Frequency-Domain Model Identification

Here, we use a frequency sweep as the pilot input, and a skilled human operator performs remote control for data collection. The flight data of inputs (control signals of servos) and outputs (the UH's attitudes, attitude rates, position, and velocities, etc.) are recorded by the Flash memory of the MGNCs at a sampling rate of 50 Hz.

To obtain a precise dynamic model of the UH, it is necessary to preprocess the input–output data, e.g., remove outliers and noise, before the data identification process. The flight data recorded by the MGNCs are separated into two subsets. One subset is used for model identification, whereas the other is used for model performance verification. Several recorded samples used for identification are shown in Fig. 6.

In this paper, we use the frequency-domain identification method. It is important to select the valid frequency range for frequency-domain identification. As we know, the coherence method is an effective tool to evaluate the quality of the sampled data [21]. Taking the lateral channel as an example, the coherence function obtained from the input–output data is shown in Fig. 7. In Fig. 7, we can see that the frequencies among 0.05–5 Hz, 8–11.5 Hz, and 14–16 Hz are superior, and the other frequencies are less significant. The cross power spectral density (CPSD) is used to further delimit the range of useful frequencies. Fig. 8 shows the CPSD values of the input and output. In Fig. 8, we can see that the CPSD values among 0.05–5 Hz are much higher than the others. In fact, the frequency of the pilot's maneuver is rarely higher than 5 Hz; therefore, 0.05–5 Hz can cover most valid frequencies. Now, we have the frequency response of the roll angular rate to lateral input, as shown in Fig. 9. The frequency response of pitch angular rate to longitudinal input is also obtained in the same way.

In what follows, we proceed to identify the model of the UH by means of the AGA presented in Section III. The parameters of the GA are not fixed, and it is very difficult to predict accurately the effects of any change in these parameters; therefore, determining their values becomes difficult [40]. Cao *et al.* [41] chose the parameters of GA using multifactor analysis of variance. Based on the method in [41], the parameters of the AGA are set as $P_{c1} = 0.85$, $P_{c2} = 0.6$, $P_{m1} = 0.1$, $P_{m2} = 0.05$, $\delta = 0.03$, $\varepsilon = 0.1$, $\alpha = 0.9$, and $\beta = 0.8$. The number for the

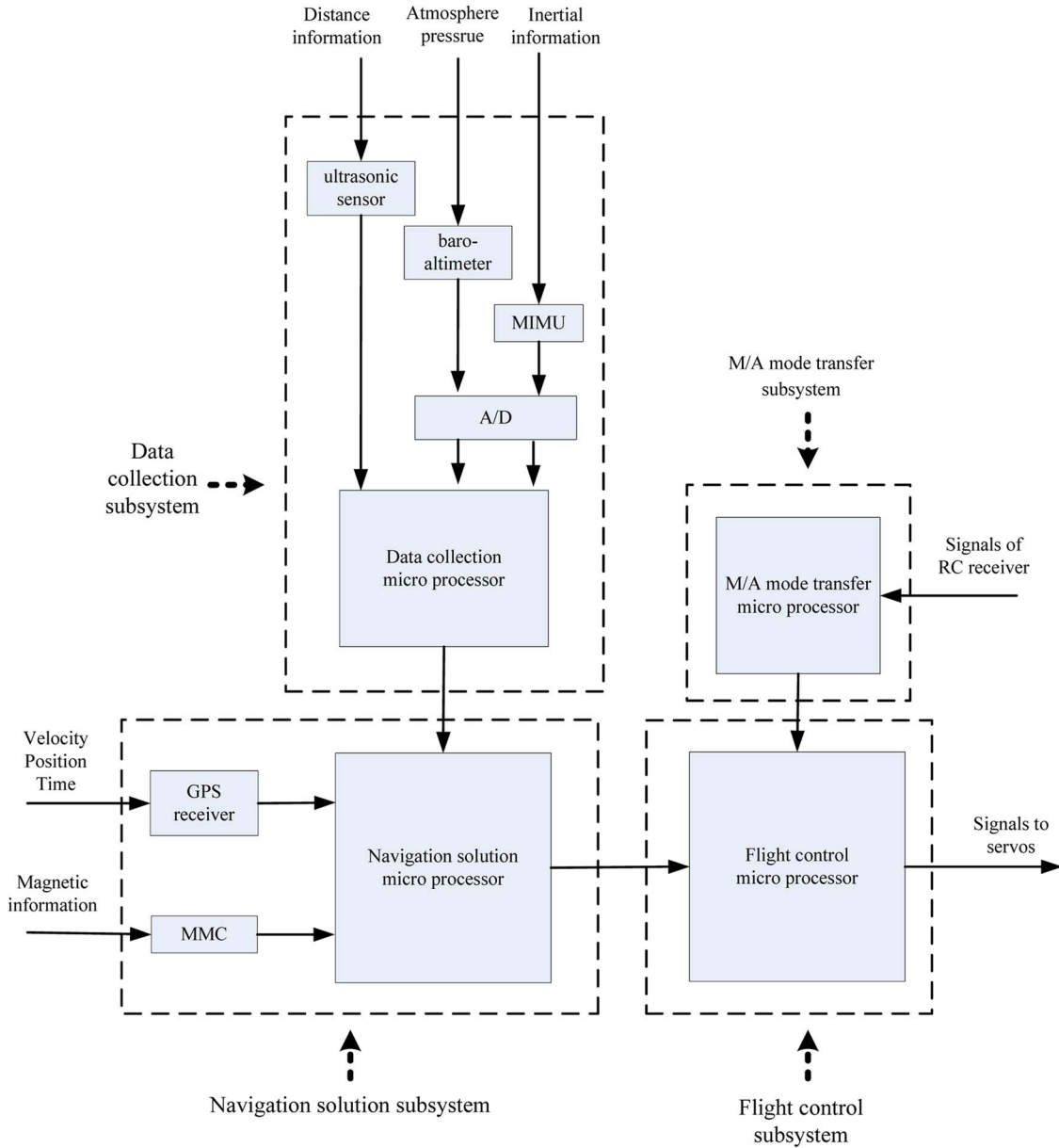


Fig. 5. Block diagram of the MGNCS.

initial population is set as 200, and the maximal offspring generation is 5000. The simple GA (SGA) is a conventional GA [32]. The selection operation of the SGA is performed on the basis of relative fitness. The crossover rate and the mutation rate of the SGA are unchanged during the whole process of computation. The performance of the AGA is tested in comparison with the SGA. The crossover rate and the mutation rate of the SGA are set as 0.8 and 0.1, respectively.

The process of identification is performed by MATLAB. The trend line of the maximum fitness value of each generation of the AGA (dotted line) in the process of identification is shown in Fig. 10. The trend line of the maximum fitness value of each generation obtained from the SGA (solid line) is also shown in Fig. 10. In Fig. 10, we can see that it is very difficult for SGA to evolve after 1000 generations, whereas the AGA evolves even after 3000 generations. It is also shown in Fig. 10 that the efficiency of the AGA in this paper is higher than that of

the SGA as the maximum fitness value of the AGA reaches 0.1789 in 500 generations and 0.2147 in 5000 generations, whereas that of SGA only reaches 0.1709 in 500 generations and 0.1732 in 5000 generations. Therefore, we can conclude that the performance of the AGA is better. Statistical tests have also been conducted to demonstrate the superiority of the AGA over the SGA. The model identification tests based on the AGA and the SGA are both carried out 30 times, and the mean values and standard errors of the identification results are shown in Table II. From Table II, we can also see that the AGA is superior to the SGA. Finally, we get the dynamic model of the UH, which is represented by

$$\begin{cases} \frac{p(z)}{w_{\text{lat}}(z)} = \frac{0.02828z^3 + 0.02634z^2 - 0.07154z + 0.005716}{z^3 - 2.434z^2 + 2.175z - 0.7092} \\ \frac{q(z)}{w_{\text{lon}}(z)} = \frac{0.1467z^3 + 0.4502z^2 - 0.6141z + 0.254}{z^3 - 2.544z^2 + 2.251z - 0.6924} \end{cases} \quad (19)$$

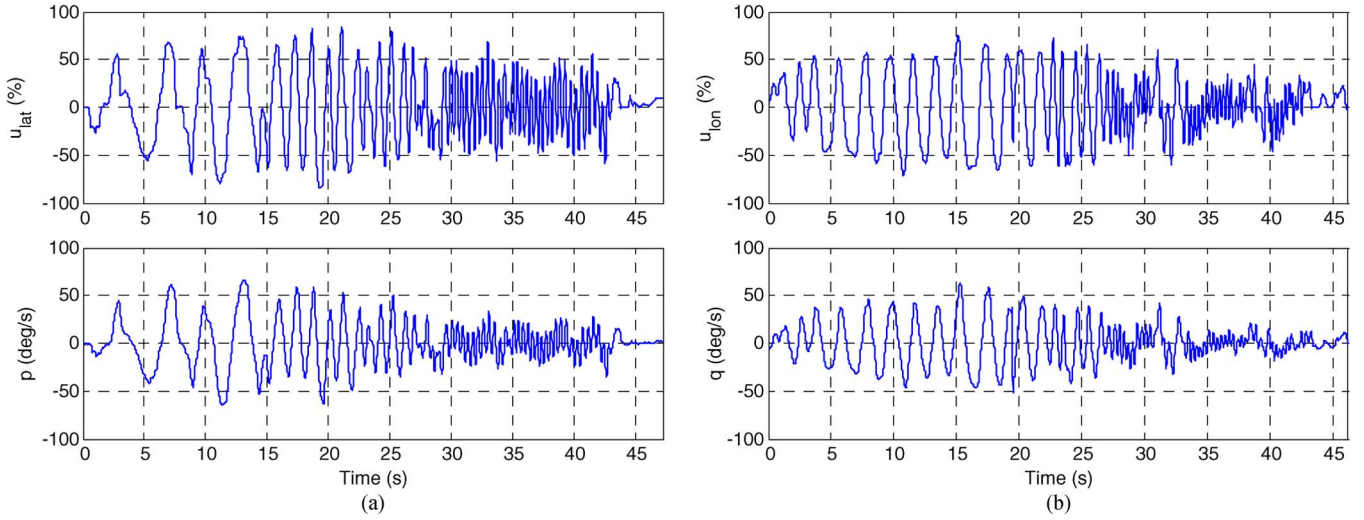


Fig. 6. Input-output data of identification. (a) Lateral channel. (b) Longitudinal channel.

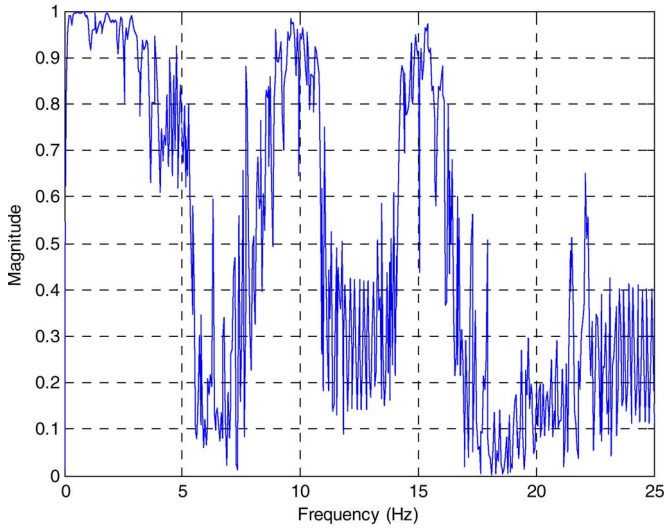


Fig. 7. Coherence function of the lateral channel.

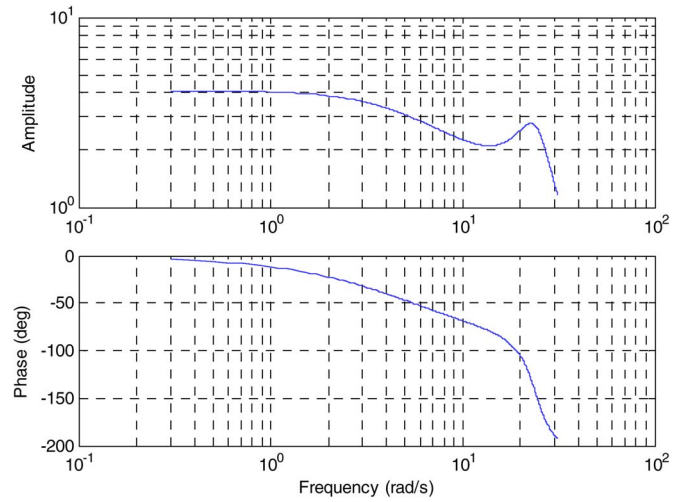


Fig. 9. Frequency response of the lateral channel.

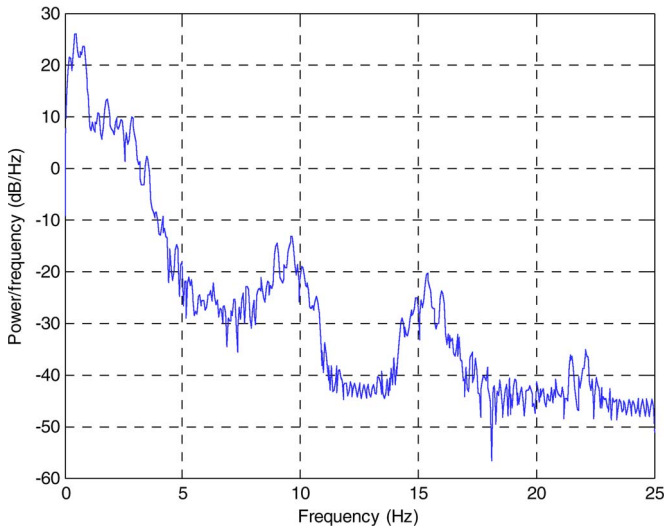


Fig. 8. CPSD of the lateral channel.

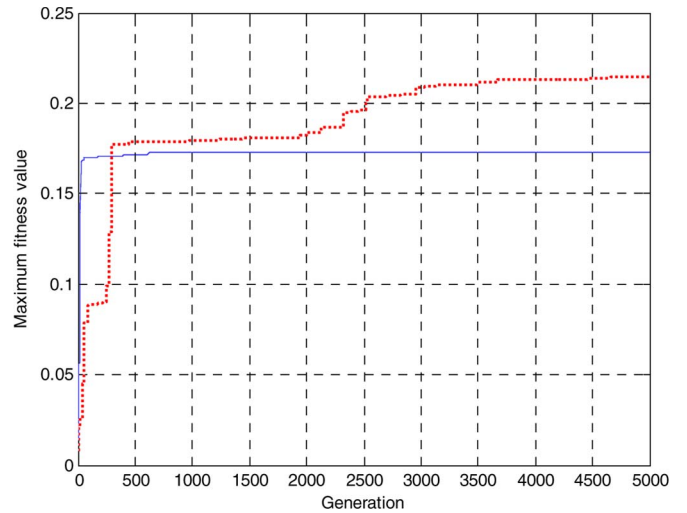


Fig. 10. Trend lines of the maximum fitness value of (dotted lines) AGA and (solid lines) SGA.

TABLE II
MEAN VALUES AND STANDARD ERRORS OF IDENTIFICATION
RESULTS BASED ON THE AGA AND THE SGA

	AGA	SGA
Mean Value	0.2031	0.1728
Standard Error	0.0005	0.0007

V. MODEL VERIFICATION

Once we obtain the identification model of the UH, it is necessary to assess its validity. In this section, a comparative study is carried out on the derived model to demonstrate the effectiveness and superiority of the frequency identification method based on the AGA.

A. Frequency-Domain and Time-Domain Verification

LS is a commonly employed identification method [31], and identification using LS has also been performed by MATLAB for comparison. The model identified from the recorded data using LS is shown in the following:

$$\begin{cases} \frac{p(z)}{u_{\text{lat}}(z)} = \frac{-0.5774z^3 + 1.3442z^2 - 0.6886z + 0.1172}{z^3 - 1.9242z^2 + 1.3542z - 0.3804} \\ \frac{q(z)}{u_{\text{lon}}(z)} = \frac{-0.9794z^3 + 2.5062z^2 - 2.0797z + 0.6602}{z^3 - 2.1984z^2 + 1.6599z - 0.4329} \end{cases} \quad (20)$$

Fig. 11 shows the frequency responses of the recorded flight data (blue solid lines) and the model obtained by the AGA (red dotted lines) and LS (black dashed lines). As shown in Fig. 11, the frequency responses obtained from the recorded data and the AGA are closely matched in terms of amplitude and phase. It can be seen that the frequency response error between the AGA and the recorded data is much smaller than that between LS and the recorded data.

In order to evaluate explicitly the frequency-domain matching degree between the recorded flight data and the identified model, the evaluation equation is adopted as follows:

$$R = 1 - \sqrt{\frac{\sum_{i=1}^N (\lambda(\omega_i) - \lambda_m(\omega_i))^2}{\sum_{i=1}^N (\lambda(\omega_i) - \bar{\lambda})^2}} \quad (21)$$

where R is the matching degree of the identified model and the real system; $\lambda(\omega_i)$ is the vector of amplitude and phase of the real system at frequency point ω_i ; $\lambda_m(\omega_i)$ is the vector of amplitude and phase of the identified model at frequency point ω_i ; and $\bar{\lambda}$ is the mean of the vectors of amplitude and phase of the real system at all of the N valid sample frequency points.

According to (21), the frequency-domain matching degree between the real flight data and the model derived from the AGA of the lateral channel is 0.8497, the matching degree between the real flight data and the model derived from LS is 0.5986, and the matching degrees of longitudinal channel under the two methods are 0.8325 and 0.5855, respectively. It is obvious that the frequency matching degrees of the identified model in (19) are much higher than those of LS.

Fig. 12 shows the time-domain verification results between the identified model in (19) and the real flight data. In Fig. 12, we can clearly see that the iterative predictive outputs of the

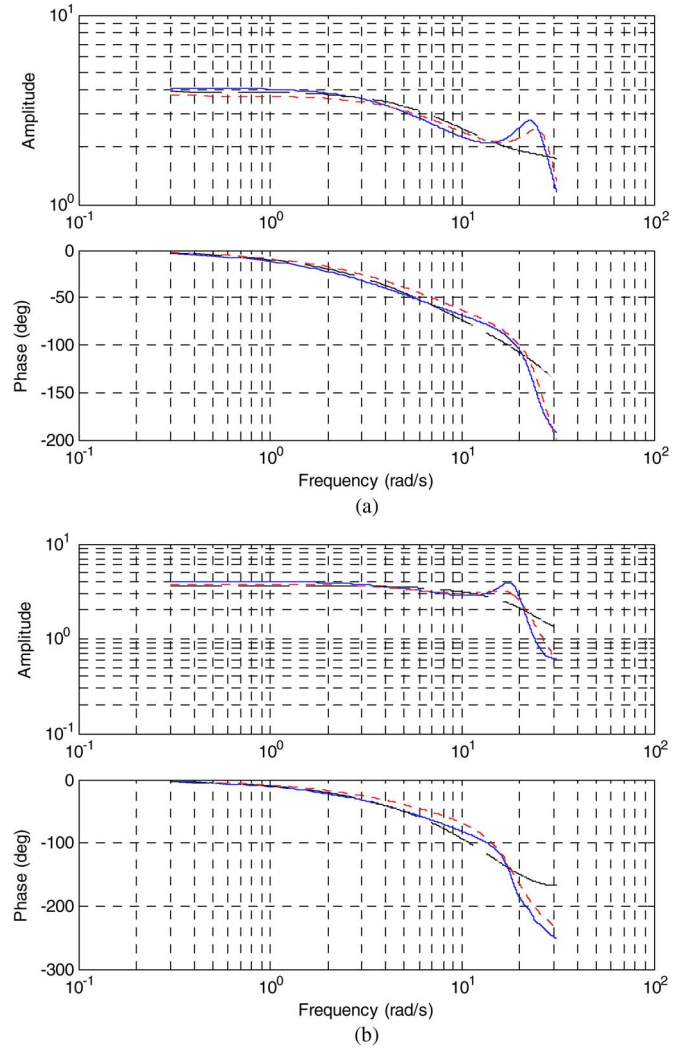


Fig. 11. Comparison of frequency responses obtained from (blue solid lines) flight data, (red dotted lines) AGA, and (black dashed lines) LS. (a) Lateral channel. (b) Longitudinal channel.

model in (19) (dotted lines) closely match the real flight data (solid lines), and the output errors are small. In fact, the matching degree of one-step-ahead predictive output is even better. Again, in order to evaluate explicitly the time-domain matching degree between the recorded flight data and the identified model, the equation below is adopted

$$R = 1 - \sqrt{\frac{\sum_{i=1}^K (y_i - y_{im})^2}{\sum_{i=1}^K (y_i - \bar{y})^2}} \quad (22)$$

where y_i is the real flight data, y_{im} is the iterative predictive output data of the identified model, \bar{y} is the mean of the real flight data, and K is the number of sample points.

According to (22), the time-domain matching degree between the real flight data and the model derived from the AGA is calculated. The matching degrees of one-step-ahead predictive output, as well as the iterative predictive output of each channel with different methods, are shown in Table III.

As shown in Table III, the time-domain matching degrees of the AGA and LS in both channels are at the same level,

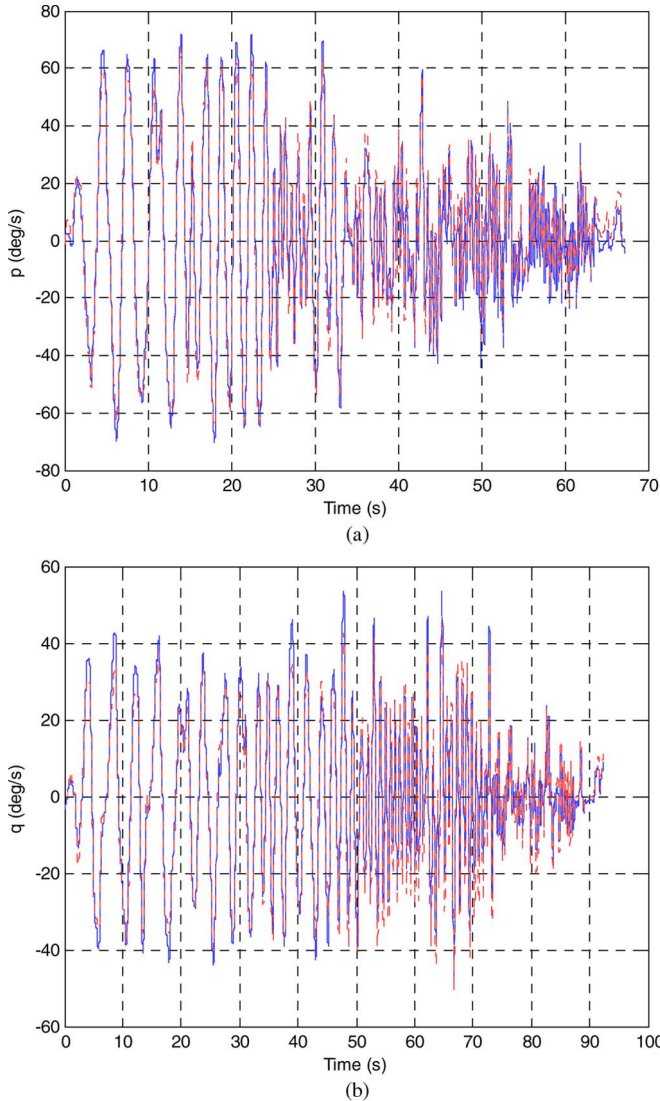


Fig. 12. Comparison of the (solid lines) measured output and iterative (dotted lines) predictive output. (a) Lateral channel. (b) Longitudinal channel.

TABLE III
TIME-DOMAIN MATCHING DEGREES OF ONE-STEP-AHEAD PREDICTIVE AND ITERATIVE PREDICTIVE OUTPUTS OF EACH CHANNEL

	AGA		LS	
	Iterative Predictive Output	One-step-ahead Predictive Output	Iterative Predictive Output	One-step-ahead Predictive Output
Lateral Channel	0.8166	0.9573	0.8152	0.9561
Longitudinal Channel	0.8155	0.9607	0.8042	0.9674

and the differences between them are not as evident as those in the frequency domain. Specifically, the matching degrees of the one-step-ahead predictive output of LS are a little higher than those of the AGA. In terms of iterative predictive output, the AGA behaves slightly better than LS in the longitudinal channel, and the result is reversed in the lateral channel.

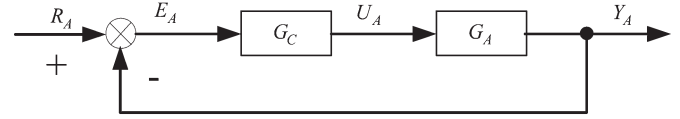


Fig. 13. Block diagram of the attitude control loop with the compensator.

B. Control Compensators Based on the Identified Model

Here, control compensators are designed based on the model identified in (19) to verify further the validity of the identification method. Comparative simulation and actual flight experiments are carried out to demonstrate the performance of the control compensators. Finally, steady automatic hovering is achieved using the compensators.

Based on the model in (19), which illustrates the relationship between the attitude rate and the input of the servo, the transfer function between the attitude and the input of the servo is derived. Wu *et al.* [14] adopted a control compensator to realize the control of the attitude loop. The block diagram of the attitude control loop with the compensator is illustrated in Fig. 13. Here, G_A is the attitude transfer function; Y_A is the attitude of the UH; R_A is the reference control attitude; E_A is the error between Y_A and R_A ; G_C is the control compensator; and U_A is the output of the control compensator. The control compensator is designed to suffice for the specifications of small overshoot and short settling time. The model-based compensation control method in [14] is utilized to select proper control compensators for the attitude control loops in this paper. The control compensators selected for the lateral and longitudinal channels based on the model of AGA are shown, respectively, in the following:

$$G_{AGA_cplat} = \frac{0.954z^2 - 4.121z + 1.602}{z^2 - z} \quad (23)$$

$$G_{AGA_cplon} = \frac{0.942z^2 - 4.01z + 1.553}{z^2 - z} \quad (24)$$

where G_{AGA_cplat} and G_{AGA_cplon} are the control compensators of lateral channel and longitudinal channel, respectively.

The control compensators selected for the lateral and longitudinal channels based on the model of LS are shown, respectively, in the following:

$$G_{cp_lat} = \frac{0.792z^2 - 3.77z + 1.523}{z^2 - z} \quad (25)$$

$$G_{cp_lon} = \frac{0.731z^2 - 3.72z + 1.51}{z^2 - z} \quad (26)$$

An attitude step reference of 30° is given to the left of the diagram of both the lateral and the longitudinal channels in Fig. 13, and the simulation control results of the model obtained from AGA and LS are shown in Fig. 14. It is shown in Fig. 14 that the overshoots of both channels of the model from AGA and LS are small.

A series of actual flight experiments are carried out on the UH to verify further the effectiveness of the control compensators derived from the identified model, and the flight data are collected by the MGNCS. The attitude control experiments of lateral and longitudinal channels are implemented separately. The UH is first maneuvered by a professional pilot, and the

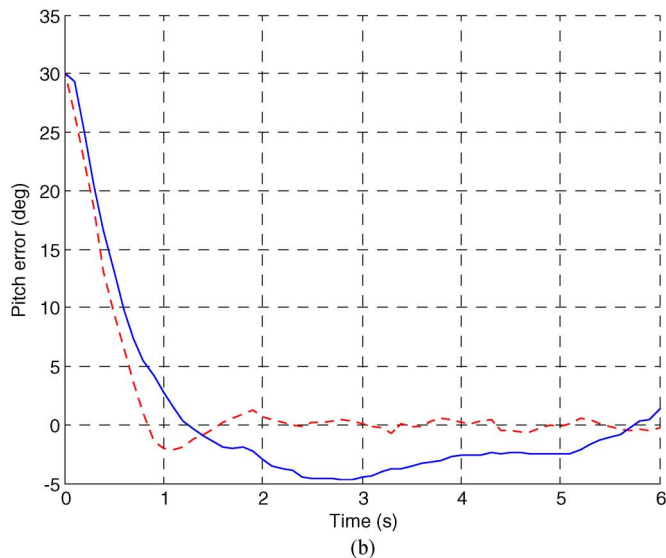
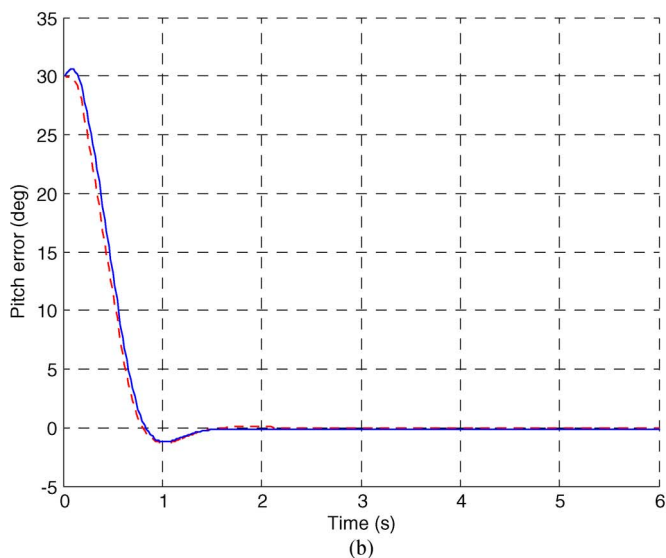
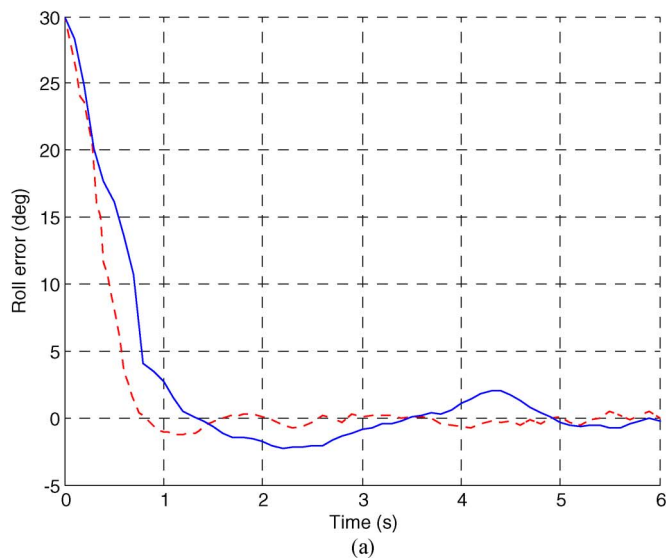
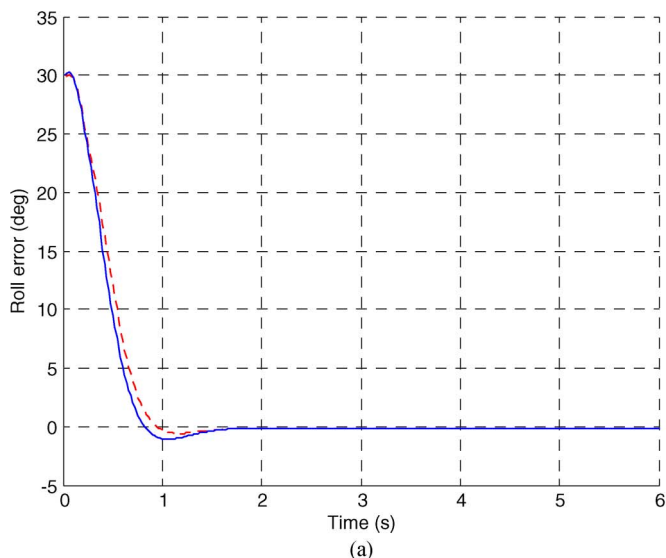


Fig. 14. Comparison of simulation attitude response errors between control loops based on (dotted lines) AGA and (solid lines) LS. (a) Lateral channel. (b) Longitudinal channel.

Fig. 15. Comparison of experimental attitude response errors between control loops based on (dotted lines) AGA and (solid lines) LS. (a) Lateral channel. (b) Longitudinal channel.

flight mode is subsequently transferred from manual mode to autonomous mode. Fig. 15(a) shows the experimental flight control results of the lateral channel. In Fig. 15(a), we can see that the roll error of the control loop based on the AGA has smaller overshoot and shorter settling time than the control loop based on LS, and the attitude fluctuation of the former is also smaller than that of the latter. In other words, it can be seen from the flight control results that the roll control loop based on the AGA is superior to that based on LS. The same conclusion can be drawn in Fig. 15(b), which displays the flight control results of the longitudinal channel.

In the following, we proceed to examine the performance of the control compensator in actual automatic hovering. The pilot manipulates the UH to the vicinity of the target point, and the flight mode of the UH is subsequently transferred from manual to autonomous mode. A number of flight tests are implemented. All of them achieved successful automatic hovering in the air. A duration of 32 s of automatic hovering is shown in Figs. 16 and 17. The horizontal coordinate of the target point is (2, 1). In

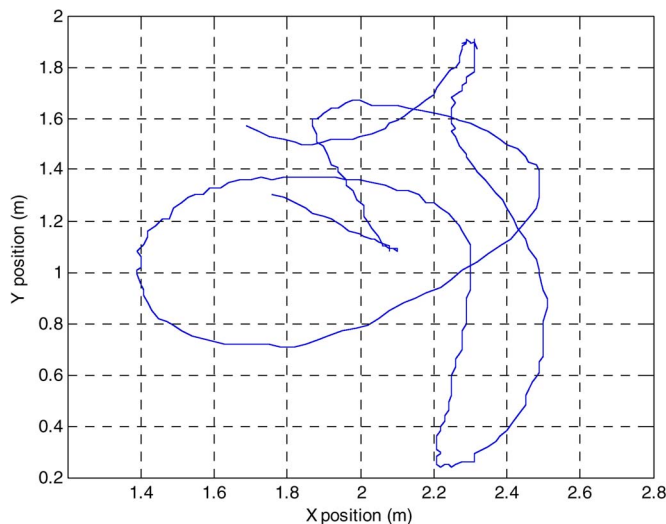


Fig. 16. Top view of the actual automatic hovering of the UH.

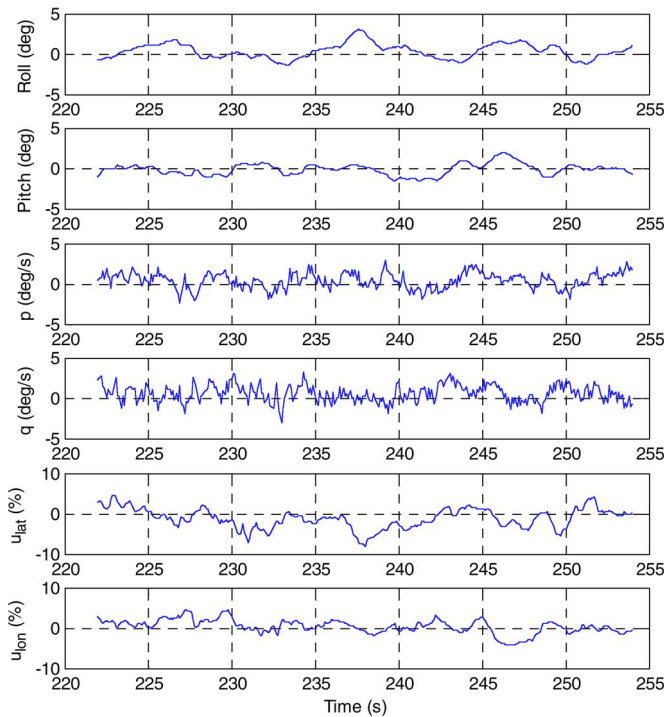


Fig. 17. Attitudes, attitude rates, and inputs of servos during the automatic hovering flight.

Fig. 16, it can be noted that the maximum horizontal tolerance in each axis is smaller than 0.9 m; specifically, it is 0.62 m in the x -direction and 0.89 m in the y -direction. This performance achieves a level 1 evaluation, according to the aeronautical design standard performance specification handling quality requirements for military rotorcraft [42]. The attitudes, attitude rates, and inputs of the servos during the automatic hovering flight are depicted in Fig. 17. It is shown in Fig. 17 that the roll and pitch of the UH are smaller than 5° , and the attitude rates are within $5^\circ/\text{s}$. It can be concluded in Figs. 16 and 17 that the control compensator designed using the identified model can successfully implement automatic hovering of the UH. The successful automatic hovering demonstrates the validity of the identified model, namely the validity and feasibility of the identification method that we designed for UH based on the AGA. It is necessary to note that good performance with a control compensator design does not necessarily mean that the system identification is perfect, as the control compensator usually bears some robustness. However, testing the performance of the controller is a common and reasonable way to test the identified model. Our further research will concentrate on the design of robust and optimal flight control methods for the UH.

VI. CONCLUSION

System identification of the UH has been carried out in this paper. The attitude model of the UH is obtained by using a frequency-domain identification method based on the AGA. Due to the superiority of the frequency-domain methods in the identification of the UH, the method in this paper shows its effectiveness and superiority in time-domain and frequency-domain analyses, compared with the commonly used identification method, i.e., LS. To verify further the performance

of the identified model, control compensators are designed using the identified model, and actual automatic hovering is successfully achieved. The simulation and experimental results demonstrate that: 1) this identification method is able to obtain a model for UH, whose effectiveness and superiority has been shown; and 2) flight controllers can be designed based on the identified model, which simplifies the design of the controller and improves the efficiency of the experimental study of the UH.

REFERENCES

- [1] R. Loh, Y. Bian, and T. Roe, "UAVs in civil airspace: Safety requirements," *IEEE Aerosp. Electron. Syst. Mag.*, vol. 24, no. 1, pp. 5–17, Jan. 2009.
- [2] B. C. Mecrow, J. W. Bennett, A. G. Jack, D. J. Atkinson, and A. J. Freeman, "Drive topologies for solar-powered aircraft," *IEEE Trans. Ind. Electron.*, vol. 57, no. 1, pp. 457–464, Jan. 2010.
- [3] G. Q. Zhou, "Geo-referencing of video flow from small low-cost civilian UAV," *IEEE Trans. Autom. Sci. Eng.*, vol. 7, no. 1, pp. 156–166, Jan. 2010.
- [4] K. Kondak, C. Deeg, G. Hommel, M. Musial, and V. Remuss, "Mechanical model and control of an autonomous small size helicopter with a stiff main rotor," in *Proc. IEEE/RSL Int. Conf. Intell. Robots Syst.*, Sendai, Japan, 2004, pp. 2469–2474.
- [5] O. Špinko, O. Holub, and Z. Hanzálek, "Low-cost reconfigurable control system for small UAVs," *IEEE Trans. Ind. Electron.*, vol. 58, no. 3, pp. 880–889, Mar. 2011.
- [6] G. W. Cai, B. M. Chen, and T. H. Lee, "An overview on development of miniature unmanned rotorcraft systems," *Front. Electron. Electron. Eng. China*, vol. 5, no. 1, pp. 1–14, 2010.
- [7] J. Ferruz, V. M. Vega, A. Ollero, and V. Blanco, "Reconfigurable control architecture for distributed systems in the HERO autonomous helicopter," *IEEE Trans. Ind. Electron.*, vol. 58, no. 12, pp. 5311–5318, Dec. 2011.
- [8] B. Zheng and Y. S. Zhong, "Robust attitude regulation of a 3-DOF helicopter benchmark: Theory and experiments," *IEEE Trans. Ind. Electron.*, vol. 58, no. 2, pp. 660–670, Feb. 2011.
- [9] J. Eckert, R. D. German, and F. Dressler, "An indoor localization framework for four-rotor flying robots using low-power sensor nodes," *IEEE Trans. Control Syst. Technol.*, vol. 60, no. 2, pp. 336–344, Feb. 2011.
- [10] F. Lin, X. Y. Dong, B. M. Chen, K. Y. Lum, and T. H. Lee, "A robust real-time embedded vision system on an unmanned rotorcraft for ground target following," *IEEE Trans. Ind. Electron.*, vol. 59, no. 2, pp. 1038–1049, Feb. 2012.
- [11] O. Tanner, "Modeling, identification, and control of autonomous helicopter," Ph.D. dissertation, Swiss Fed. Inst. Technol., Zurich, Switzerland, 2003.
- [12] L. Marconi and R. Naldi, "Robust full degree-of-freedom tracking control of a helicopter," *Automatica*, vol. 43, no. 11, pp. 1909–1920, Nov. 2007.
- [13] D. Park, M. S. Park, and S. K. Hong, "A study on the 3-DOF attitude control of free-flying vehicle," in *Proc. IEEE Int. Symp. Ind. Electron.*, Pusan, Korea, 2001, pp. 1260–1265.
- [14] H. Y. Wu, D. Sun, and Z. Y. Zhou, "Model identification of a micro air vehicle in loitering flight based on attitude performance evaluation," *IEEE Trans. Robot.*, vol. 20, no. 4, pp. 702–712, Aug. 2004.
- [15] G. L. Wang, H. Xia, and J. H. Zhu, "Time-domain model identification of a small-scale unmanned helicopter," in *Proc. 30th Chinese Control Conf.*, Yantai, China, 2011, pp. 1647–1651.
- [16] G. W. Cai, B. M. Chen, K. M. Peng, M. B. Dong, and T. H. Lee, "Modeling and control of the yaw channel of a UAV helicopter," *IEEE Trans. Ind. Electron.*, vol. 55, no. 9, pp. 3426–3434, Sep. 2008.
- [17] A. Budiyo, K. J. Yoon, and F. D. Daniel, "Integrated identification modeling of rotorcraft-based unmanned aerial vehicle," in *Proc. 17th Mediterranean Conf. Control Autom.*, Thessaloniki, Greece, 2009, pp. 898–903.
- [18] H. B. Qian, G. Q. Chang, H. X. Chang, and Y. P. Yang, "A grey-modeling research on a small-scale autonomous helicopter," in *Proc. Int. Conf. Inf. Eng. Comput. Sci.*, 2009, pp. 1–4.
- [19] E. D. Beckmann and G. A. Borges, "Nonlinear modeling, identification and control for a simulated miniature helicopter," in *Proc. IEEE Latin Amer. Robot. Symp.*, 2008, pp. 53–58.
- [20] M. Manai, A. Desbiens, and E. Gagnon, "Identification of a UAV and design of a hardware-in-the-loop system for nonlinear control purposes," in *Proc. AIAA Guid. Navig. Control Conf. Exhib.*, San Francisco, CA, USA, 2005, pp. 6483–6488.

- [21] B. Mettler, *Identification Modeling and Characteristics of Miniature Rotorcraft*. Norwell, MA, USA: Kluwer, 2003, pp. 55–137.
- [22] M. B. Tischler and M. G. Cauffman, “Frequency-response method for rotorcraft system identification: Flight applications to BO-105 coupled fuselage/rotor Dynamics,” *J. Amer. Helicopter Soc.*, vol. 37, pp. 3–17, 1992.
- [23] B. Mettler, “Modeling small-scale unmanned rotorcraft for advanced flight control design,” Ph.D. dissertation, Carnegie Mellon Univ., Pittsburgh, PA, USA, 2001.
- [24] B. Mettler, T. Kanade, and M. B. Tischler, “System identification modeling of a model-scale helicopter,” Robotics Inst., Carnegie Mellon Univ., Pittsburgh, PA, USA, Rep. CMU-RI-TR-00-03, Jan. 2000.
- [25] B. Mettler, T. Kanade, M. B. Tischler, and W. Messner, “Attitude control optimization for a small-scale unmanned helicopter,” in *Proc. AIAA Guid. Navig. Control Conf. Exhib.*, Denver, CO, USA, 2000, pp. 1–10.
- [26] B. Mettler, M. B. Tischler, and T. Kanade, “System identification of small-size unmanned helicopter dynamics,” in *Proc. Amer. Helicopter Soc. 55th Forum*, Montreal, QC, Canada, 1999, pp. 1–25.
- [27] J. Nino, F. Mittrache, P. Cosyn, and R. de Keyser, “Model identification of a micro air vehicle,” *J. Bionic Eng.*, vol. 4, no. 4, pp. 227–236, Dec. 2007.
- [28] S. H. Chung and H. K. Chan, “A two-level genetic algorithm to determine production frequencies for economic lot scheduling problem,” *IEEE Trans. Ind. Electron.*, vol. 59, no. 1, pp. 611–619, Jan. 2012.
- [29] C. C. Tsai, H. C. Huang, and C. K. Chan, “Parallel elite genetic algorithm and its application to global path planning for autonomous robot navigation,” *IEEE Trans. Ind. Electron.*, vol. 58, no. 10, pp. 4813–4821, Oct. 2011.
- [30] X. S. Lei and Y. H. Du, “A linear domain system identification for small unmanned aerial rotorcraft based on adaptive genetic algorithm,” *J. Bionic Eng.*, vol. 7, no. 2, pp. 142–149, Jun. 2010.
- [31] Jategaonkar, V. Ravindra, and F. K. Lu, *Flight Vehicle System Identification: A Time Domain Methodology*. Reston, VA, USA: Amer. Inst. Aeronaut. Astron., Inc., 2006, pp. 178–187.
- [32] Z. Michalewicz, C. Z. Janikow, and J. B. Krawczyk, “A modified genetic algorithm for optimal control problems,” *Comput. Math. Appl.*, vol. 23, no. 12, pp. 83–94, Jun. 1992.
- [33] S. N. Sivanandam and S. N. Dz, *Introduction to Genetic Algorithms*. Berlin, Germany: Springer-Verlag, 2008, pp. 15–81.
- [34] X. B. Cao, Z. Zheng, K. S. Liu, and X. F. Wang, “Research on quadratic assignment problem using an immune evolution strategy,” *Computer Eng.*, vol. 26, no. 3, pp. 1–3, Mar. 2000.
- [35] X. Zhang and J. C. Fang, “A design of low power, high capability GNC System of micro unmanned aerial vehicle,” in *Proc. AIAA Guid. Navig. Control Conf. Exhib.*, San Francisco, CA, USA, 2005, pp. 1–11.
- [36] J. C. Fang and J. L. Li, “Integrated model and compensation of thermal errors of silicon microelectromechanical gyroscope,” *IEEE Trans. Instrum. Meas.*, vol. 58, no. 9, pp. 2923–2930, Sep. 2009.
- [37] J. C. Fang, H. W. Sun, J. J. Cao, X. Zhang, and Y. Tao, “A novel calibration method of magnetic compass based on ellipsoid fitting,” *IEEE Trans. Instrum. Meas.*, vol. 60, no. 6, pp. 2053–2061, Jun. 2011.
- [38] J. C. Fang and X. L. Gong, “Predictive iterated Kalman filter for INS/GPS integration and its application to SAR motion compensation,” *IEEE Trans. Instrum. Meas.*, vol. 59, no. 4, pp. 909–915, Apr. 2010.
- [39] J. S. Bendat and A. G. Piersol, *Engineering Applications of Correlation and Spectral Analysis*. New York, NY, USA: Wiley-Interscience, 1980.
- [40] C. F. Tsai and K. M. Chao, “The contingent design for the optimal parameter settings of genetic algorithms,” in *Proc. IEEE 12th Int. Conf. Comput. Supported Cooperative Work Des.*, Xi’an, China, 2008, pp. 217–222.
- [41] Z. F. Cao and Z. H. Zhang, “Parameter settings of genetic algorithm based on multi-factor analysis of variance,” in *Proc. IEEE 4th Int. Conf. Genetic Evol. Comput.*, Shenzhen, China, 2010, pp. 305–307.
- [42] *Aeronautical Design Standard Performance Specification Handling Qualities Requirements for Military Rotorcraft*, U.S. Army Aviation Missile Command, Huntsville, AL, USA, ADS-33E-PRF, 2000.



Yuhu Du was born in Shandong, China, in 1982. He received the B.S. and M.S. degrees from the Air Force Engineering University, Xi’an, China, in 2004 and 2008, respectively. He is currently working toward the Ph.D. degree at Beihang University, Beijing, China.

His main research interests include novel inertial instrument and equipment technology, model identification, and control and navigation technology of unmanned aerial vehicles.

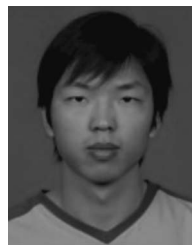


Jiancheng Fang (M’12) was born in September 1965. He received the B.S. degree from Shandong University of Technology (now Shandong University), Jinan, China, in 1983, the M.S. degree from Xi’an Jiaotong University, Xi’an, China, in 1988, and the Ph.D. degree from Southeast University, Nanjing, China, in 1996.

He is currently the Dean of the School of Instrumentation Science and Optoelectronics Engineering, Beihang University, Beijing, China. He is the author or coauthor of over 150 papers and four books. He

is the holder of 35 Chinese invention patents. His current research interests include the attitude control system technology of spacecraft, novel inertial instrument and equipment technology, inertial navigation, and integrated navigation technology of aerial vehicles.

Dr. Fang has the special appointment professorship with the title of “Cheung Kong Scholar,” which has been jointly established by the Ministry of Education of China and the Li Ka Shing Foundation. He is in the first group of Principal Scientists of the National Laboratory for Aeronautics and Astronautics of China. He was a recipient of the first-class National Science and Technology Progress Award of China as the Third Contributor in 2006, the first-class National Invention Award of China as the First Inventor, and the second-class National Science and Technology Progress Award of China as the First Contributor in 2007.



Cunxiao Miao was born in 1981 in Fujian, China. He received the B.S. degree from Northeast University, Shenyang, China, in 2006 and the Ph.D. degree from Beihang University, Beijing, China, in 2013.

He is currently a Lecturer with the School of Mechanical Engineering, University of Science and Technology Beijing, Beijing. His research interests include navigation, identification, and control of unmanned aerial vehicles.